Ultrasonics 96 (2019) 232–239

Contents lists available at ScienceDirect

Ultrasonics

journal homepage: www.elsevier.com/locate/ultras

Creeping motion characteristics due to bulk wave excitation in an elastic half-space

Pankaj Kumar[a,*], Anirvan DasGupta[a,b], Ranjan Bhattacharyya[a]

[a] Department of Mechanical Engineering, IIT Kharagpur, Kharagpur 721302, India
[b] Centre for Theoretical Studies, IIT Kharagpur, Kharagpur 721302, India

ARTICLE INFO

Keywords:
Bulk wave
Creeping motion
Interface impedance
Friction
Preload

ABSTRACT

In this work, the contact problem between a preloaded rigid surface against a restrained elastic half-space is considered under wave excitation. The half-space is assumed to be bonded imperfectly to the rigid surface, and subjected to external tractions and bulk waves. Under incident bulk wave excitation at the contact, we study the creeping motion of the preloaded rigid surface. Two possible local regions at the interface are considered, namely slip region, and region of separation, which are described by the corresponding boundary conditions and inequalities at the interface. With these considerations, creeping motion characteristics and interface conditions are obtained analytically and discussed. The effects of interface imperfection, wave parameters, and preload tractions are studied numerically. The creeping motion is found to be affected significantly by nature of the imperfection. In addition, creep motion is also analyzed considering friction at the interface. These aspects have potential applications in ultrasonic devices for micro-positioning and micro-motion control.

1. Introduction

The area of micro-positioning and micro-motion control of objects and granular materials using propagating waves is of considerable research interest [1–4]. Material handling and transportation in many industries (such as pharmaceutical and food processing) use vibratory transport in feeders, conveyors and gravity-driven silos etc. Such devices employ transverse linear or elliptical motion of the base for transport [5,6]. The application of progressive waves and vibration for fine manipulation, transport, and segregation of granular materials has been proposed in the past [7–10]. Under high frequency excitation (close to ultrasonic frequency), a fundamental problem is to understand the interaction at the interface of two bodies. In this work, we consider a flat rigid surface in imperfect contact with an elastic half-space. One of the interesting application of this work is in wave induced creeping motion and transport. This motivates the present work.

In the past research, the interface boundary is treated to be either fixed or free. In some recent studies, wave scattering has been analyzed in the presence of tangential slip at an interface, and such interface is commonly known as imperfect or weakly bonded interface. With this setting, detailed studies of wave responses including its reflection-refraction and dispersion response were presented by the several authors. In the isotropic and homogeneous elastic media, a study of attenuation and dispersion of Stoneley wave at an imperfect interface has been discussed in [11]. Reflection/refraction and attenuation of body waves and associated energetics at an imperfect interface have been considered by Murty [12]. The wave motion characteristics in the presence of such imperfect interface have been analyzed in several contexts, e.g., the transmission of waves in a saturated porous solid placed on an elastic half-space [13], in the piezoelectric/piezomagnetic media [14–16]. The harmonics generation in the presence of imperfect interface is observed both theoretically and experimentally by Nam et al. [17], where the authors analyze the reflection and refraction of incident bulk waves with different interfacial stiffnesses. In practice, in presence of such contact conditions, the propagating wave with induced shear traction at the driving interface can develop drift along the propagation. Therefore, if an object is unrestrained, it can exhibit creeping motion with respect to the other restrained object. Such motion can occur with or without preload tractions.

Although previous studies showed that imperfect interface could strongly affect the wave fields intensity and its behavior, most of this investigation is based on grounded substrates, and thus, our current understanding of how this imperfection exhibits a drift along the interface is still limited. Also, under such contact conditions, the investigated wave interaction systems mostly have a uniform behavior of the interface. However, the boundary conditions in this situation allow the unrestrained body to slide and separate locally with partial transmission of the active fields. Such a boundary can exhibit properties of

* Corresponding author.
E-mail addresses: pankaj.kekti@gmail.com (P. Kumar), anir@mech.iitkgp.ernet.in (A. DasGupta), rbmail@mech.iitkgp.ernet.in (R. Bhattacharyya).

https://doi.org/10.1016/j.ultras.2019.01.001
Received 20 September 2018; Received in revised form 17 December 2018; Accepted 5 January 2019
Available online 14 January 2019
0041-624X/ © 2019 Elsevier B.V. All rights reserved.

sliding interface. The gap formation and its effects on interfacial tractions due to imperfection have not been well analyzed and reported. The present solution method, therefore, considers such wave induced separation and examines the creeping motion for understanding the sliding behavior and the complex interface behavior.

Normally, the sliding interface associated with the wave propagation problem is modeled considering friction at the interface. The propagation of elastic wave in the presence of unilateral boundary with localized gap formation is studied by Comninou and Dundurs [18,19]. They investigated the steady sliding of an unrestrained medium, and also observed the change in phase of reflected/refracted waves. These ideas are extended in [20,21] to analyze the excitation of in-plane waves due to out-of-plane waves, and vice versa, using an iterative procedure. A similar problem of friction interface in a sandwich structure is analyzed in [22] using Fourier analysis. The excitation of body waves in presence of frictional boundary is considered and studied by Adams [23], and Nosonovsky and Adams [24]. The formulation is used further in [25] to analyze the reflected/refracted waves without considering the harmonics generation. The interaction of elastic waves and its energetics at the frictional boundary with sliding condition has been analyzed recently by Watanabe [26] considering the Doppler effect.

In the presence of the frictional/imperfect interface, the previous studies mostly concentrate on the determination of amplitude and energy ratios; such as the effects of wave parameters and friction coefficient on reflection/refraction coefficients and energy partition. Relatively fewer studies have investigated the induced motion assisted by an incoming wave and its beneficial outcomes. A correction technique based on the superposition of the secondary solution is used in this work. The analysis of such system having a frictional/imperfect interface is of importance in both theoretical and practical studies of ultrasonics.

In this work, we consider the wave induced motion of a preloaded rigid surface, i.e., the rigid surface is driven by the strong incident bulk wave against the grounded half-space. We assume the half-space to be a homogeneous and isotropic elastic solid, and subjected to an incidence wave field at the interface. Further, we consider that the rigid surface is having infinite elastic moduli, and hence, it doesn't deform under wave excitation and preload tractions. Also, the thickness is unimportant in describing such surface. We solve the elastodynamic problem through a solution correction technique, as proposed by Comninou and Dundurs [18,19], taking into account both imperfect and frictional interface. The creeping motions are analytically analyzed for the case of imperfect interface. In this case, a displacement jump is considered at the interface with an assumption that the slip and interface shear traction are linearly dependent. The frictional interface problem is considered as a second case of this formulation. In the analysis, the frequency shift and harmonics generation in the reflected waves are neglected. The variations of the drift velocity with the incidence wave, interface impedance parameter and preloads are determined and studied. It is observed that, the rigid surface creeps with respect to the half-space with possible slip/stick bands at the interface. In both the cases, an interfacial gap may form which depends mainly upon the preloads.

2. Problem formulation

Consider an elastic half-space having density ρ, with longitudinal and transverse wave velocities as c_L and c_T, respectively. The half-space is connected to a rigid base at its flat horizontal boundary as shown schematically in Fig. 1. In the initial bilateral problem, the common boundary is assumed to be rigidly fixed. Hence, the system of waves in the half-space must satisfy the condition of vanishing displacements at the boundary initially. At $x_2 = 0$, the incoming P-wave is reflected as P- and SV-wave in the half-space. Also, we assume that the incidence P-wave is having an angular frequency ω, and is making an angle θ with the boundary normal. The displacement fields in the half-space

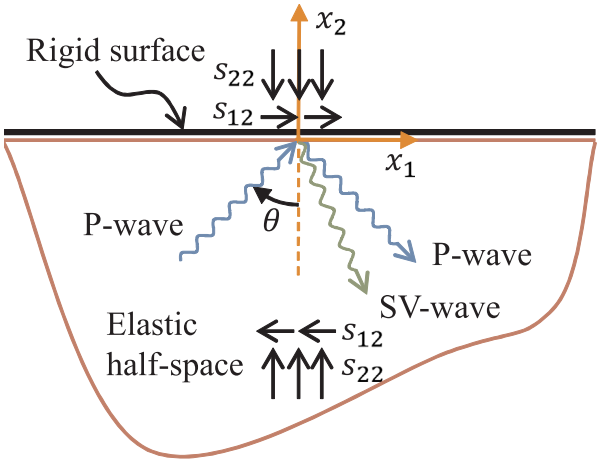

Fig. 1. Schematic of present investigation, an elastic half-space held imperfectly/frictionally against a rigid surface, a system of waves along with the coordinates.

comprising the longitudinal and transverse fields are given by

$$u_1 = [A_1 k e^{ik\alpha x_2} + A_2 k e^{-ik\alpha x_2} + B_2 k\beta e^{-ik\beta x_2}]e^{ik(x_1 - ct)}, \tag{1a}$$

$$u_2 = [A_1 k\alpha e^{ik\alpha x_2} - A_2 k\alpha e^{-ik\alpha x_2} + B_2 k e^{-ik\beta x_2}]e^{ik(x_1 - ct)}, \tag{1b}$$

where k is horizontal wave number of incoming wave. The phase velocity is $c = \omega/k$, and A_1, A_2 and B_2 are the incident P-wave, reflected P- and SV-wave amplitude, respectively, and

$$\alpha^2 = \left(\frac{c^2}{c_L^2} - 1\right), \quad \beta^2 = \left(\frac{c^2}{c_T^2} - 1\right).$$

Using Eqs. (1a) and (1b), the stress fields are obtained from Hooke's law as

$$\sigma_{12} = [2iA_1 k^2\alpha\mu e^{ik\alpha x_2} - 2iA_2 k^2\alpha\mu e^{-ik\alpha x_2} - iB_2 k^2(\beta^2 - 1)\mu e^{-ik\beta x_2}]e^{ik(x_1 - ct)}, \tag{2a}$$

$$\sigma_{22} = [iA_1 k^2(\lambda + \alpha^2\lambda + 2\alpha^2\mu)e^{ik\alpha x_2} + iA_2 k^2(\lambda + \alpha^2\lambda + 2\alpha^2\mu)e^{-ik\alpha x_2} - 2iB_2 k^2\beta\mu e^{-ik\beta x_2}]e^{ik(x_1 - ct)}, \tag{2b}$$

where λ and μ are the Lamé coefficients. For bilateral interface, i.e., the vanishing displacement boundary $\mathbf{u}|_{x_2=0} = 0$, the reflected wave amplitudes are obtained from Eqs. (1a) and (1b) as

$$A_2 = \left(\frac{\alpha\beta - 1}{\alpha\beta + 1}\right)A_1, \quad B_2 = \left(\frac{-2\alpha}{\alpha\beta + 1}\right)A_1.$$

Substituting above in Eqs. (2a) and (2b), one can rewrite the stress fields at $x_2 = 0$ by taking the real part as

$$\sigma_{12}|_{x_2=0} = \left[\frac{-2k^2\alpha\mu(1 + \beta^2)}{\alpha\beta + 1}\right]A_1 \sin[k(x_1 - ct)], \tag{3a}$$

$$\sigma_{22}|_{x_2=0} = \left[\frac{-2k^2\beta(\alpha + \alpha^3)(\lambda + 2\mu)}{\alpha\beta + 1}\right]A_1 \sin[k(x_1 - ct)]. \tag{3b}$$

A convenient approach to establish the solution of the present problem is to correct the wave fields in initially assumed bilateral problem. For corrected solutions, the wave amplitudes are, in general, complex to begin with. Hence, the amplitudes A_2 and B_2 in displacement and stress fields Eqs. (1) and (2) are replaced with complex amplitudes $A_2' = (C_1' + iD_1')$ and $B_2' = (C_2' + iD_2')$, respectively, without loss of generality. Further, the primed notations $\mathbf{u}'$, σ_{12}' and σ_{22}' refer to corresponding displacement and stress fields. Here, the frequency shift and harmonics generation in the reflected waves are neglected. Now, both the solutions are superimposed in order to meet the boundary conditions at the interface of actual problem. Therefore, the total stress

fields at the interface $x_2 = 0$ can be written as

$$S_{12}(x_1, t)|_{x_2=0} = s_{12} + \sigma_{12}|_{x_2=0} + \sigma'_{12}|_{x_2=0}, \tag{4a}$$

$$S_{22}(x_1, t)|_{x_2=0} = -s_{22} + \sigma_{22}|_{x_2=0} + \sigma'_{22}|_{x_2=0}, \tag{4b}$$

where the first terms in Eqs. (4a) and (4b) are the distributed preloads, applied externally (see Fig. 1). The preloads are considered small in comparison to the stress fields in bilateral solution. Writing the propagator term as $\xi = k(x_1 - ct)$, and using (3) in (4) yields on simplification the interfacial stress fields

$$S_{12}(\xi) = s_{12} + a\sin\xi + \sum_{j=1}^{2} m_j [C'_j \sin\xi + D'_j \cos\xi], \tag{5a}$$

$$S_{22}(\xi) = -s_{22} + b\sin\xi + \sum_{j=1}^{2} n_j [C'_j \sin\xi + D'_j \cos\xi], \tag{5b}$$

where

$$a = \left[\frac{-2k^2\alpha\mu(1+\beta^2)}{\alpha\beta+1}\right]A_1,$$
$$b = \left[\frac{-2k^2\beta(\alpha+\alpha^3)(\lambda+2\mu)}{\alpha\beta+1}\right]A_1,$$

and

$$m_j = \begin{cases} 2k^2\alpha\mu, & j = 1 \\ k^2(\beta^2 - 1)\mu, & j = 2 \end{cases},$$
$$n_j = \begin{cases} -k^2(\lambda + \alpha^2\lambda + 2\alpha^2\mu), & j = 1 \\ 2k^2\beta\mu, & j = 2 \end{cases}.$$

It is considered that the incoming wave is strong enough so that interfacial slip can occur at the common boundary due to velocity mismatch. The interfacial slip fields we used are given by the difference in velocity between the rigid surface and the elastic half-space both in longitudinal and transverse directions. Here, the slip fields at the interface are obtained by differentiating the displacement fields for the corrected solution as

$$V_1(\xi) = v_0 - \dot{u}'_1 = v_0 + k^2 c \sum_{j=1}^{2} m'_j [C'_j \sin\xi + D'_j \cos\xi], \tag{6a}$$

$$V_2(\xi) = -\dot{u}'_2 = k^2 c \sum_{j=1}^{2} n'_j [C'_j \sin\xi + D'_j \cos\xi], \tag{6b}$$

where v_0 is the rigid body drift velocity in positive x_1 direction, and

$$m'_j = \begin{cases} -1, & j = 1 \\ -\beta, & j = 2 \end{cases}, \quad n'_j = \begin{cases} \alpha, & j = 1 \\ -1, & j = 2 \end{cases}.$$

One can combine the Eqs. (5) and (6) by eliminating the summation terms as

$$S_{12}(\xi) = s_{12} + a\sin\xi + E_{11}[V_1^\star(\xi) - v_0^\star] + E_{12}V_2^\star(\xi), \tag{7a}$$

$$S_{22}(\xi) = -s_{22} + b\sin\xi + E_{21}[V_1^\star(\xi) - v_0^\star] + E_{22}V_2^\star(\xi), \tag{7b}$$

where $V_j^\star(\xi) = V_j(\xi)/k^2c$, $v_0^\star = v_0/k^2c$, and

$$E_{ij} = \begin{bmatrix} m_1 & m_2 \\ n_1 & n_2 \end{bmatrix}\begin{bmatrix} m'_1 & m'_2 \\ n'_1 & n'_2 \end{bmatrix}^{-1},$$

are the components of matrix E.

2.1. Solution for imperfect interface

This case considers a basic assumption that the interface stress fields are linearly dependent to the slip fields. The different proportionality constants in the assumption refer to the measure of imperfection. Hence, in deriving the drift velocity characteristics, we will require the following boundary condition at the interface

$$S_{12}(\xi) = K[V_1(\xi)],$$

where K is the parameter representing the imperfection in the longitudinal direction, and is known as *surface flow impedance*. Further, we rearrange and rewrite the above boundary condition using a mapped constant $\phi = (1 - \phi)(Kc/\mu)$ as follows

$$S_{12}(\xi) = \frac{\phi}{1-\phi}k^2\mu[V_1^\star(\xi)]. \tag{8}$$

For the condition $\phi = 0$, the shear stress vanishes, and similarly, the condition $\phi = 1$ leads to zero tangential slip field at the interface. The interfacial gap is developed at the boundary due to the assumed strong incoming wave. The gap is defined as the difference in transverse displacements between the two bodies. The magnitude and extension of the gap are controlled by the normal preload. Now, for such a local gap, the half-space looses contact with the base, and hence, the stress fields vanish. Then, the condition $\phi = 0$ yields

$$S_{12}(\xi) = 0, \quad S_{22}(\xi) = 0. \tag{9}$$

The gap $g(\xi) \geq 0$ and its variation with moving coordinate ξ can be obtained by choosing the weaker form as

$$g(\xi) = -k\int V_2^\star(\xi)d\xi. \tag{10}$$

Using (9) in (7), we solve for $V_2^\star$. Substituting the expression of $V_2^\star$ in Eq. (10) and integrating, we obtain

$$g(\xi) = \frac{-k}{E_{11}E_{22} - E_{12}E_{21}}[s_{12}E_{21}\xi + s_{22}E_{11}\xi - (aE_{21} - bE_{11})\cos\xi + C], \tag{11}$$

where C is the constant of integration. The gap extended in the region $\xi \in (g_l, g_r)$, and the right interfacial gap boundary ($g_r > \pi/2$) can be found using (9) in (7) and substituting $V_2^\star(\xi) = 0$ as

$$\sin g_r = \frac{s_{12}E_{21} + s_{22}E_{11}}{bE_{11} - aE_{21}}. \tag{12}$$

The left boundary g_l is determined by vanishing gap condition and using the constant C in Eq. (11). Further, the gap is confirmed by a resulting negative normal traction in the slip region. This is discussed numerically in Section 3. Now we consider the slip condition at the interface. The stress field $S_{12}(\xi)$ must satisfy the linear relationship Eq. (8) in the slip region along with the following conditions

$$g(\xi) = 0, \quad S_{22}(\xi) \leqslant 0. \tag{13}$$

Now, the tangential slip fields in the two regions are calculated as

$$V_1^\star = \begin{cases} v_0^\star + F_{11}(-s_{12} - a\sin\xi) + F_{12}(s_{22} - b\sin\xi), & \xi \in (g_l, g_r) \\ \left(E_{11} - \frac{\phi}{1-\phi}k^2\mu\right)^{-1}(E_{11}v_0^\star - s_{12} - a\sin\xi), & \\ \xi \in [-\pi, g_l) \text{and} (g_r, \pi] & \end{cases}, \tag{14}$$

where the matrix F is calculated as

$$F = [m'_1 \;\; m'_2]\begin{bmatrix} m_1 & m_2 \\ n_1 & n_2 \end{bmatrix}^{-1}.$$

It may be noted that the problem is periodic in ξ. Hence, we consider $\xi \in [-\pi, \pi]$. The drift velocity is hence calculated by integrating Eq. (14) over the indicative period of ξ. Using Eq. (14b) in Eq. (7), and vanishing normal slip condition $V_2^\star = 0$, one can obtain the interfacial traction fields as

$$S_{12}(\xi)=$$
$$\begin{cases} 0, \ \xi \in (g_l, g_r) \\ s_{12} + a\sin\xi + E_{11}[(E_{11} - (\phi/(1-\phi))k^2\mu)^{-1} \\ \times(E_{11}v_0^\star - s_{12} - a\sin\xi) - v_0^\star], \ \xi \in [-\pi, g_l) \text{ and } (g_r, \pi] \end{cases},$$
$$S_{22}(\xi)=$$
$$\begin{cases} 0, \ \xi \in (g_l, g_r) \\ -s_{22} + b\sin\xi + E_{21}[(E_{11} - (\phi/(1-\phi))k^2\mu)^{-1} \\ \times(E_{11}v_0^\star - s_{12} - a\sin\xi) - v_0^\star], \ \xi \in [-\pi, g_l) \text{ and } (g_r, \pi] \end{cases}. \quad (15)$$

2.2. Solution for frictional interface

Let us consider the half-space interacting frictionally with the rigid base. Assume, for simplicity, that both the kinetic and static friction coefficients are to be equal. One can then write the frictional interface boundary conditions in the following form

$$S_{12}(\xi) = \begin{cases} -\nu S_{22}(\xi), & S_{12}(\xi) > 0 \\ \nu S_{22}(\xi), & S_{12}(\xi) < 0 \end{cases}, \quad (16)$$

where ν is the friction coefficient. The calculation of gap and its extension can be performed similarly as discussed in the previous case. The normal slip field $V_2(\xi)$ is zero everywhere except over the gap region, and hence the boundary conditions (16) can be rearranged and written using Eq. (7) as

$$s_{12} + a\sin\xi + E_{11}[V_1^\star(\xi) - v_0^\star]=$$
$$\begin{cases} -\nu[-s_{22} + b\sin\xi + E_{21}[V_1^\star(\xi) - v_0^\star]], & S_{12}(\xi) > 0 \\ \nu[-s_{22} + b\sin\xi + E_{21}[V_1^\star(\xi) - v_0^\star]], & S_{12}(\xi) < 0 \end{cases}. \quad (17)$$

Let the slip region in the interface be denoted by (s_{li}, s_{ri}) with $i = 1$ and 2 for left and right slip regions, respectively. The tangential slip field $V_1^\star(\xi)$ is zero at the slip boundaries for the gap isolated with a slip region. Then, using the above conditions, one can calculate the boundaries of slip regions from Eq. (16) as

$$(a + \nu b)\sin s_{l2} = -s_{12} + \nu s_{22} + (E_{11} + \nu E_{21})v_0^\star, \quad (18a)$$

$$(a - \nu b)\sin s_{r1} = -s_{12} - \nu s_{22} + (E_{11} - \nu E_{21})v_0^\star, \quad (18b)$$

followed by the following periodic conditions

$$s_{l2} + s_{r2} = \pi, \quad s_{l1} + s_{r1} = -\pi.$$

The region outside the slip and gap region is known as the *stick region*. Also, the field $V_1^\star(\xi)$ vanishes in the stick region. Finally, after some algebra, the slip field $V_1^\star(\xi)$ for frictional interface case is obtained as

$$V_1^\star(\xi)=$$
$$\begin{cases} v_0^\star + F_{11}(-s_{12} - a\sin\xi) \\ \quad + F_{12}(s_{22} - b\sin\xi), & \xi \in (g_l, g_r) \\ v_0^\star + (E_{11} - \nu E_{21})^{-1}[-s_{12} \\ -a\sin\xi + \nu(-s_{22} + b\sin\xi)], & \xi \in (s_{l1}, s_{r1}) \\ v_0^\star + (E_{11} + \nu E_{21})^{-1}[-s_{12} \\ -a\sin\xi - \nu(-s_{22} + b\sin\xi)], & \xi \in (s_{l2}, g_l) \text{ and } (g_r, s_{r2}) \\ 0, & \xi \in [-\pi, s_{l1}), (s_{r1}, s_{l2}) \\ & \text{and } (s_{r2}\pi] \end{cases} \quad (19)$$

Integrating Eq. (19) over ξ in the interval $[-\pi, \pi]$ yields the corresponding drift velocity in this case. It may be noted that the different regions mentioned above can also disappear depending on the values of the different parameters. The traction fields are obtained using Eqs. (7) and (19) as

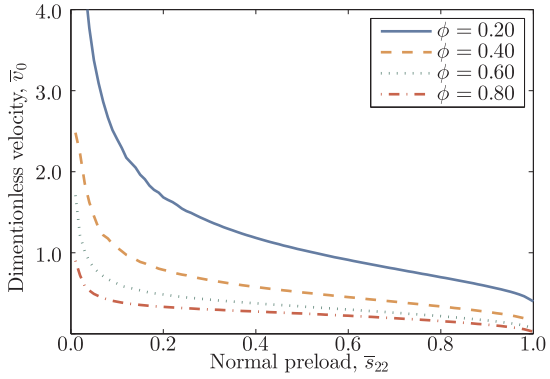

(a)

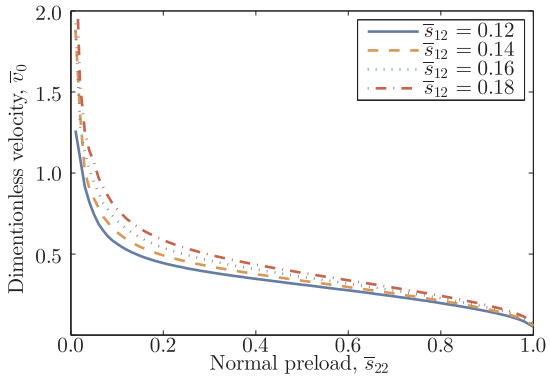

(b)

Fig. 2. The drift velocity variation as function of normal preload $\bar{s}_{22}$ for imperfect interface condition: (a) for selected values of parameter ϕ and at shear preload value $\bar{s}_{12} = 0.1$; (b) for selected values of preload $\bar{s}_{12}$ and at interface impedance parameter value $\phi = 0.7$.

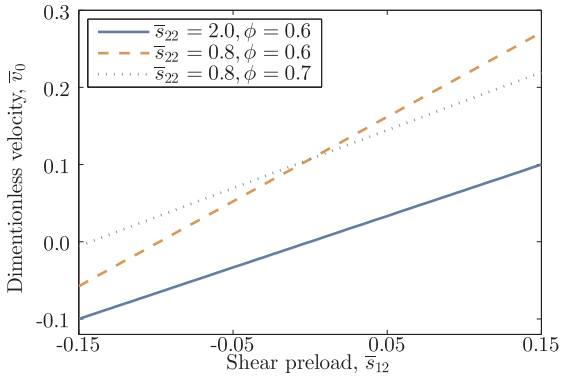

Fig. 3. The drift velocity variation as function of shear preload $\bar{s}_{12}$ for imperfect interface condition for selected values of preload $\bar{s}_{22}$ and parameter ϕ.

Table 1
Extent of different regions at the imperfect interface for the one period of ξ.

No.	Parameters values ($\bar{s}_{12}$, $\bar{s}_{22}$, ϕ)	g_l	g_r	$\bar{v}_0$
1	0.10, 0.60, 0.60	− 0.3702	2.4932	0.2986
2	0.10, 0.60, 0.80	− 0.3702	2.4932	0.2220
3	0.10, 0.80, 0.80	0.2728	2.2058	0.1563
4	0.00, 0.80, 0.80	0.2708	2.2067	0.1070
5	− 0.10, 0.80, 0.80	0.2687	2.2077	0.0577
6	0.10, 2.00, 0.60	...	...	0.0667

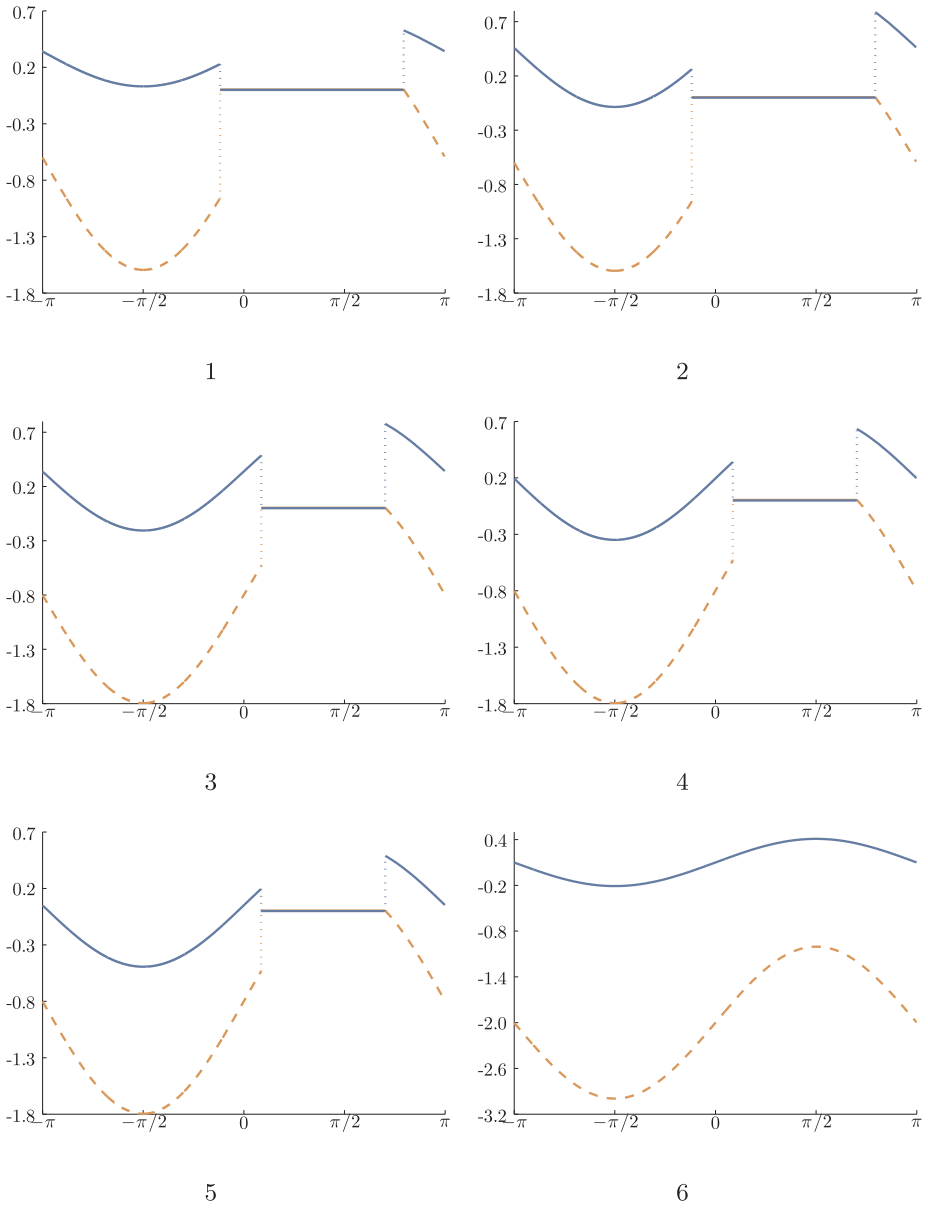

Fig. 4. The variation of shear traction $\bar{S}_{12}$ (*blue solid line*), and normal traction $\bar{S}_{22}$ *(orange dashed line)* for one period of ξ, the selected parameters are listed in Table 1, and corresponding row numbers are displayed in sub-caption. (For interpretation of the references to color in this figure legend, the reader is referred to the web version of this article.)

$$S_{12}(\xi) = \begin{cases} 0,\ \xi \in (g_l,\, g_r) \\ s_{12} + a\sin\xi + E_{11}(E_{11} - \nu E_{21})^{-1} \\ \times [-s_{12} - a\sin\xi + \nu(-s_{22} + b\sin\xi)],\ \xi \in (s_{l1},\, s_{r1}) \\ s_{12} + a\sin\xi + E_{11}(E_{11} + \nu E_{21})^{-1} \\ \times [-s_{12} - a\sin\xi - \nu(-s_{22} + b\sin\xi)],\ \xi \in (s_{l2},\, g_l) \text{ and } (g_r,\, s_{r2}) \\ s_{12} + a\sin\xi + E_{11}(-v_0^{\star}),\ \xi \in [-\pi,\, s_{l1}),\ (s_{r1},\, s_{l2}) \text{ and } (s_{r2},\, \pi] \end{cases} \tag{20a}$$

$$S_{22}(\xi) = \begin{cases} 0,\ \xi \in (g_l,\, g_r) \\ -s_{22} + b\sin\xi + E_{21}(E_{11} - \nu E_{21})^{-1} \\ \times [-s_{12} - a\sin\xi + \nu(-s_{22} + b\sin\xi)],\ \xi \in (s_{l1},\, s_{r1}) \\ -s_{22} + b\sin\xi + E_{21}(E_{11} + \nu E_{21})^{-1} \\ \times [-s_{12} - a\sin\xi - \nu(-s_{22} + b\sin\xi)],\ \xi \in (s_{l2},\, g_l) \text{ and } (g_r,\, s_{r2}) \\ -s_{22} + b\sin\xi + E_{21}(-v_0^{\star}),\ \xi \in [-\pi,\, s_{l1}),\ (s_{r1},\, s_{l2}) \text{ and } (s_{r2},\, \pi] \end{cases} \tag{20b}$$

3. Results and discussion

The creep motion derived above is now calculated numerically and demonstrated, and the effects of the different parameters of the incidence wave and interface are studied. The creep motion is measured through the drift velocity. With respect to an observer situated on the rigid surface, the elastic half-space will appear to be moving in the opposite direction with the same speed. The present analysis considers an incoming P-wave within its sub-critical incidence. We consider a half-space made of steel having density $\rho = 7800\ \mathrm{kg\ m^{-3}}$, and wave speeds $c_L = 6020.18\ \mathrm{m\ s^{-1}}$, $c_T = 3217.92\ \mathrm{m\ s^{-1}}$, which is extended infinitely in negative x_2 direction (see Fig. 1). A speed independent interface impedance parameter and friction is considered [25]. The following dimensionless quantities, $\bar{v}_0 = v_0^{\star} k^2 \mu / a$, $\bar{s}_{12} = s_{12}/a$, $\bar{s}_{22} = s_{22}/b$, are introduced.

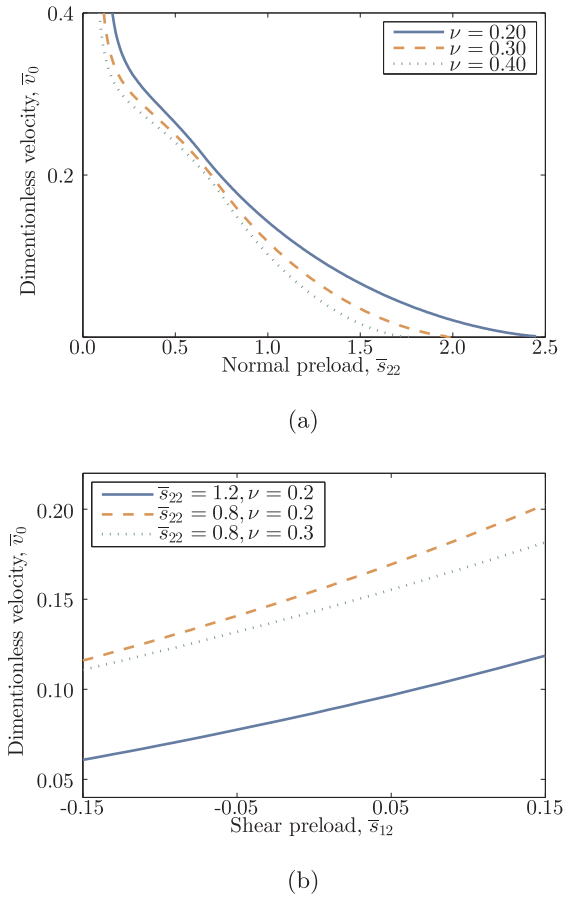

Fig. 5. The drift velocity variation for frictional interface: (a) as function of normal preload $\bar{s}_{22}$ for selected values of coefficient ν and at shear preload value $\bar{s}_{12} = 0.1$; (b) as function of shear preload $\bar{s}_{12}$ for selected values of preload $\bar{s}_{22}$ and coefficient ν.

Table 2
Extent of different regions at the frictional interface for the one period of ξ.

No.	Parameters values ($\bar{s}_{12}$, $\bar{s}_{22}$, ν)	s_{l2}	g_l	g_r	s_{r2}	$\bar{v}_0$
1.	0.10, 0.60, 0.20	− 0.2760	− 0.3702	2.4932	− 2.8656	0.2386
2.	0.10, 0.80, 0.30	0.0959	0.2728	2.2058	3.0457	0.1681
3.	− 0.10, 0.80, 0.30	0.2712	0.2687	2.2077	2.8704	0.1211
4.	0.10, 2.00, 0.20	0.8322	...	...	2.3094	0.0207

3.1. Half-space connected imperfectly to a rigid base

We begin with the calculation of the gap and its extension, as discussed in Section 2.1. A similar approach is presented by Comninou and Dundurs in [18] for a loosely bonded interface between two half-spaces. Figure 2 shows the variation of the dimensionless drift velocity $\bar{v}_0$ with the applied normal preload $\bar{s}_{22}$ for incidence angle $\theta = 30°$ under imperfect interface condition. In Fig. 2a the variations are plotted for a constant shear preload $\bar{s}_{12} = 0.1$, and for certain values of interface impedance parameter ϕ in the range [0, 1]. The variation of drift velocity is found to be monotonic with the applied normal preload $\bar{s}_{22}$. Also, the velocity decreases as the parameter ϕ increases for fixed preload values $\bar{s}_{22}$. In order to interpret the sliding behavior with external shear, we presented the velocity variation for certain shear preload values in Fig. 2b. The drift velocity is found to increase with the increase in shear preload. An increase of the interface impedance parameter ϕ implies a reduction in the tangential displacement mismatch. Using this aspect, one can explain why the velocity decreases with increase in the parameter ϕ. For the situation when gap vanishes, the velocities are expected to have constant amplitudes. This can be described by the condition of zero normal slip field at the interface.

The drift velocity response with the shear preload for the imperfect interface is plotted in Fig. 3 for three different cases. The velocity increases almost linearly with $\bar{s}_{12}$. It is observed that a positive drift is possible even for negative or zero shear preload. This corresponds to the pure wave excited drift motion. The increase in shear in the opposite direction causes an increase in velocity in the negative direction. It can also be observed that, at certain values of shear preload, creep motion is completely arrested.

Table 1 lists the some possible coordinates of gap and slip regions at the interface for couple of sets of parameters. The incidence angle is considered to be fixed at 30°. Since the bonding get always stronger when the parameter ϕ increases, the drift velocity of the rigid surface always decreases (see rows 1 and 2 in Table 1). Also, it is observed that the gap region extension is free from interface impedance parameter ϕ. Further, for the higher normal preloads the gap region shrinks and the drift velocity decreases (see rows 2 and 3 in Table 1). In the above analysis, a positive velocity is observed without being subjected to shear preloads and even for negative shear preloads, and is presented in rows 4 and 5 in Table 1. Then, as discussed previously, a positive velocity is observed in row 6 in Table 1 for condition $\bar{s}_{22} \geq 1$, for which the gap is not present.

The non-dimensional interface tractions $\bar{S}_{12} = S_{12}(\xi)/a$, and $\bar{S}_{22} = S_{22}(\xi)/b$ are computed and plotted in Fig. 4. The sub-caption numbers in the figures are the corresponding row numbers of Table 1. It is evident that the shear fields can have variations in both positive and negative directions. However, the normal fields vary in the negative direction only. Also, the traction fields are zero valued at the gap region in all the cases. For normal traction fields, there is a discontinuity in traction occurs at the left boundary of the gap $\xi = g_l$. In a similar manner, the shear fields show discontinuity at both the boundaries of the gap at $\xi = g_l$ and g_r (see Fig. 4). The primary reason for the left discontinuity is the normal preload, while the right discontinuity contribution in shear field variations is due to the parameter ϕ. In the absence of shear preload s_{12}, and for $\phi = 0$, we observe from Eq. (8) that $S_{12}(\xi) = 0$, i.e., the net shear field will disappear, and the slip field $V_2(\xi)$ at the interface will vanish if the gap is vanished. This implies that the interface becomes perfectly smooth, and the drift velocity tends to infinity.

In comparison with the previous results, in this case, the discontinuity in the shear fields are observed at the right end of the separation region. This is caused due to the nature of surface flow impedance parameter ϕ. Also, in the particular cases when $\phi = 0$, or $\phi = 1$, the present results reduce to the results obtained previously for limiting cases of smooth or adhesive interface in [20,21].

3.2. Half-space connected frictionally to a rigid base

In the second problem with a frictional interface, the drift velocities are obtained for an incidence angle of 30°. A partially similar problem has been analyzed by somewhat different approach in Comninou and Dundurs [19]. Fig. 5a and b show the velocity variation with the normal and shear preload, respectively. In Fig. 5a, the variation is presented graphically for different frictional coefficients ν at $\bar{s}_{12} = 0.1$. It is observed that the velocity decreases with the increase in coefficient ν for any arbitrary fixed preload values $\bar{s}_{12}$ and $\bar{s}_{22}$. Also, the variation is less sensitive to the coefficient ν for small normal preload values. We have plotted the distribution of drift velocity with the shear preload $\bar{s}_{12}$ in Fig. 5b. It is observed that the velocity increases approximate linearly with $\bar{s}_{12}$. Here, the trend behaves oppositely to the previous variation. The dimensionless velocity $\bar{v}_0$ is observed to stay positive even for small negative shear preload. Also, the velocities are tend to have negative direction for large negative $\bar{s}_{12}$ and for smaller ν values.

The data in Table 2 presented some possible arrangements of

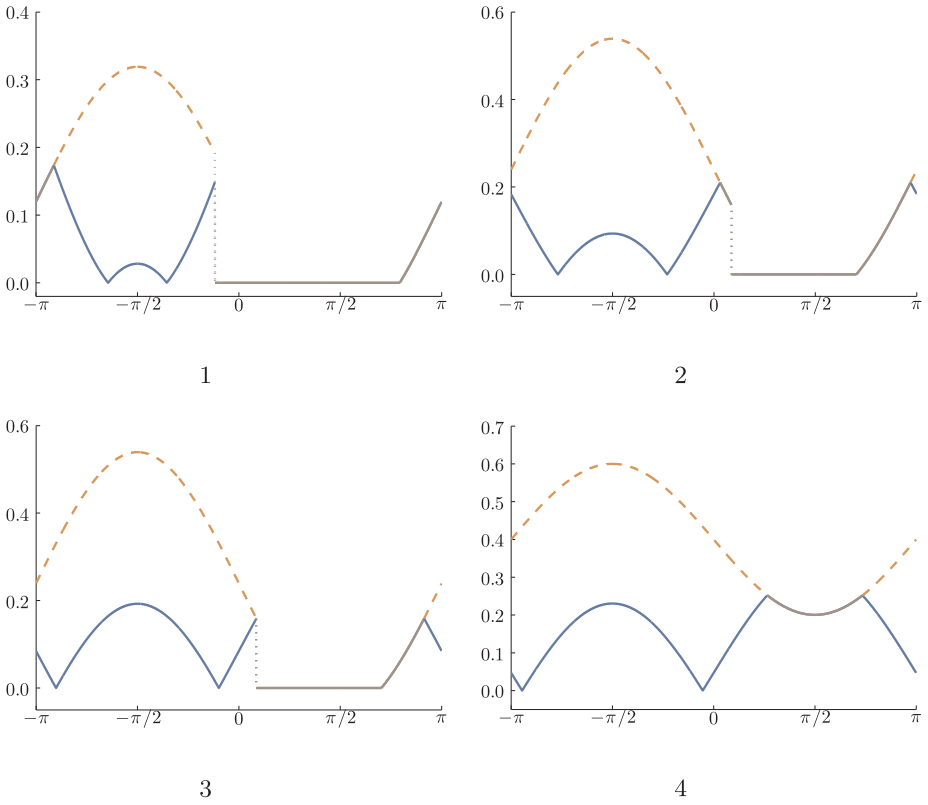

Fig. 6. The variation of quantities $|\overline{S}_{12}(\xi)|$ (*blue solid line*), and $\nu|\overline{S}_{22}(\xi)|$ (*orange dashed line*) for one period of ξ, the selected parameters are listed in Table 2, and corresponding row numbers are displayed in sub-caption. (For interpretation of the references to color in this figure legend, the reader is referred to the web version of this article.)

coordinates of local interfacial regions in this case. It is noted that the left slip regions (s_{l1}, s_{r1}) are not observed for the selected parameters and wave type, and hence it is excluded. As in the previous case, here also the separation region is independent of coefficient ν. Further, the negative values of s_{r2} in few cases mean that the right slip region is continued outside the right boundary of ξ. Here, the quantities $|\overline{S}_{12}(\xi)| = |S_{12}(\xi)/a|$, and $\nu|\overline{S}_{22}(\xi)| = \nu|S_{22}(\xi)/a|$ are computed and depicted in Fig. 6. The sub-caption numbers are same as the corresponding rows of Table 2. The tractions are zero valued in the gap region similar to the case of imperfect interface discussed previously. Unlike the previous case, here both the traction fields show discontinuity only at the boundary $\xi = g_l$. Further, it can easily observed from Fig. 6 that the solution satisfying the interfacial boundary conditions $|\overline{S}_{12}(\xi)| = \nu|\overline{S}_{22}(\xi)|$ at slip region, and similarly $|\overline{S}_{12}(\xi)| < \nu|\overline{S}_{22}(\xi)|$ at stick region, which are quite evident.

In the absence of friction, somewhat similar trends of interfacial tractions at the interface of two elastic half-space has been noticed, as studied by Comninou and Dundurs [18]. Some results and observations are partly reflected in their study.

4. Conclusions

In this analytical study, we have introduce a surface flow impedance parameter to study the effect of an incidence elastic wave on an imperfect interface. The closed-form solution for drift velocity is obtained using the solution correction method. The effects of external preloads and interface impedance parameter on the creeping motion characteristics are analytically explored and discussed. The drift motion is observed to reduce with increase in the interface impedance parameter due to decrease in the displacement mismatch. The limiting case of a smooth interface is easily achieved when the net shear traction is made to vanish. To compare the different conditions and inequalities at the interface, the results are also obtained under variation of interface tractions.

For the specific case of frictional interface, the effects of frictional coefficients on drift velocity and interface tractions are also examined analytically and discussed. It is found that the velocity increases almost linearly with shear preload. In addition, it is also possible to obtain a negative drift velocity with higher negative shear preload along with higher friction coefficient or with lower interface impedance parameter.

The present work addresses the drift motion actuated by bulk waves. Localized loss of contact, and stick-slip behavior have been considered. The study is relevant for understanding the creeping motion characteristics induced at such sliding interfaces. The analysis can be extended further with consideration of surface waves. Also, the frequency shift and harmonics generation in the reflected waves can be examined.

Declaration of interest

None.

References

[1] T. Takano, Y. Tomikawa, Excitation of a progressive wave in a lossy ultrasonic transmission line and an application to a powder-feeding device, Smart Mater. Struct. 7 (1998) 417–421.
[2] M. Mracek, J. Wallaschek, A system for powder transport based on piezoelectrically excited ultrasonic progressive waves, Mater. Chem. Phys. 90 (2005) 378–380.
[3] B.-G. Loh, P.I. Ro, An object transport system using flexural ultrasonic progressive waves generated by two-mode excitation, IEEE Trans. Ultrason. Ferroelectr. Frequency Control 47 (2000) 994–999.
[4] R. Gabai, D. Ilssar, R. Shaham, N. Cohen, I. Bucher, A rotational traveling wave based levitation device–modelling, design, and control, Sens. Actuators A Phys. 255 (2017) 34–45.
[5] K. Erdesz, A. Szalay, Experimental study on the vibrational transport of bulk solids, Powder Technol. 55 (1988) 87–96.
[6] E. Sloot, N.P. Kruyt, Theoretical and experimental study of the transport of granular

materials by inclined vibratory conveyors, Powder Technol. 87 (1996) 203–210.
[7] W. Hall, J. Beddow, Ultrasonic vibration in sieving, Ultrasonics 7 (1969) 154.
[8] N. Verma, A. DasGupta, Particle current on flexible surfaces excited by harmonic waves, Phys. Rev. E 88 (2013) 052915.
[9] J. Hu, Acoustic micro/nano manipulations: an editorial review, Int. J. Radiol. 1 (2014) 1–3.
[10] G. Ruhela, A. DasGupta, Hopping on a wave: from periodic to chaotic transport, Nonlinear Dyn. 86 (2016) 1663–1672.
[11] G.S. Murty, A theoretical model for the attenuation and dispersion of Stoneley waves at the loosely bonded interface of elastic half spaces, Phys. Earth Planet. Inter. 11 (1975) 65–79.
[12] G.S. Murty, Reflection, transmission and attenuation of elastic waves at a loosely-bonded interface of two half spaces, Geophys. J. Int. 44 (1976) 389–404.
[13] A.K. Vashisth, M.D. Sharma, M.L. Gogna, Reflection and transmission of elastic waves at a loosely bonded interface between an elastic solid and liquid-saturated porous solid, Geophys. J. Int. 105 (1991) 601–617.
[14] Y. Pang, J.-X. Liu, Reflection and transmission of plane waves at an imperfectly bonded interface between piezoelectric and piezomagnetic media, Eur. J. Mech. A/Solids 30 (2011) 731–740.
[15] W.-H. Sun, G.-L. Ju, J.-W. Pan, Y.-D. Li, Effects of the imperfect interface and piezoelectric/piezomagnetic stiffening on the SH wave in a multiferroic composite, Ultrasonics 51 (2011) 831–838.
[16] G. Nie, J. Liu, X. Fang, Z. An, Shear horizontal (SH) waves propagating in piezoelectric–piezomagnetic bilayer system with an imperfect interface, Acta Mech. 223 (2012) 1999–2009.
[17] T. Nam, T. Lee, C. Kim, K.-Y. Jhang, N. Kim, Harmonic generation of an obliquely incident ultrasonic wave in solid–solid contact interfaces, Ultrasonics 52 (2012) 778–783.
[18] M. Comninou, J. Dundurs, Reflexion and refraction of elastic waves in presence of separation, Proc. Roy. Soc. Lond. A 356 (1977) 509–528.
[19] M. Comninou, J. Dundurs, Interaction of elastic waves with a unilateral interface, Proc. Roy. Soc. Lond. A 368 (1979) 141–154.
[20] Y.-S. Wang, G.-L. Yu, Re-polarization of elastic waves at a frictional contact interface–II. Incidence of a P or SV wave, Int. J. Solids Struct. 36 (1999) 4563–4586.
[21] Y.-S. Wang, G.-L. Yu, H.-H. Dai, Transmission of elastic waves through a frictional contact interface between two anisotropic dissimilar media, Wave Motion 37 (2003) 137–156.
[22] P. Kumar, A. DasGupta, R. Bhattacharyya, Wave induced sliding at the interface between a layered elastic medium and a half-space, Meccanica 53 (2018) 3399–3413.
[23] G.G. Adams, Radiation of body waves induced by the sliding of an elastic half-space against a rigid surface, J. Appl. Mech. 67 (2000) 1–5.
[24] M. Nosonovsky, G.G. Adams, Dilatational and shear waves induced by the frictional sliding of two elastic half-spaces, Int. J. Eng. Sci. 39 (2001) 1257–1269.
[25] M. Nosonovsky, G.G. Adams, Interaction of elastic dilatational and shear waves with a frictional sliding interface, J. Vib. Acoust. 124 (2002) 33–39.
[26] K. Watanabe, Elastodynamic doppler effects and wave energy partition by a sliding interface, Acta Mech. 228 (2017) 4169–4186.